Supporting Information

Koval et al. 10.1073/pnas.0913760107

SI Text

SI Materials and Methods. ***Ventricular myocyte isolation and viral infection.*** Adult male New Zealand white rabbits (1.5–2 kg) were anesthetized by sodium pentobarbital (50 mg/mL) with Heparin (55 units/mL) through i.v. injection (1 mL/1 kg). Hearts were excised, perfused retroaortically (Langendorff), and enzymatically digested with a mixture of collagenase (Type 2) (Worthington, 250 units/mL), hyaluronidase (Sigma, 0.01%), and protease Type XIV (Sigma, 0.0025%) in a modified Tyrode's solution (0.1 mM CaCl2, 10 mM BDM). Dissociated cardiomyocytes were washed three times in Joklik MEM (Sigma) with 1% Pen/Strep and 1X ITS (Sigma) with increasing Ca^{2+} (0.25, 0.5, 0.75 mM). Ventricular myocytes were plated on glass coverslips (glass #1) coated with Geltrex (Invitrogen, thin layer) and allowed to attach for 1 h. Cells were washed with a culture media consisting of a 50:50 mix of DMEM and F10 media with 1% Pen/Strep and 1X ITS. Attached cardiomyocytes were counted and the cell density was calculated. Multiplicity of infection was 1–3 viral particles per cell.

β-subunits. The open reading frame of rat β_{2a} (accession no. NM_053851.1) with an N-terminal FLAG tag was amplified by PCR, as described (1), and ligated into the adenoviral vector pacAd5CMVmcsIRESeGFPpA (Gene Transfer Vector Core at the University of Iowa, GTVC). The β_{2a} mutants were created by using the QuikChange Mutagenesis Kit, essentially as described by the manufacturer (Stratagene). The identities of all mutant and WT cDNA sequences were confirmed by sequencing.

CaMKII, constitutively active CaMKII and CaMKII inhibition. We inhibited CaMKII activity by two approaches. We expressed the neuronal endogenous CaMKII inhibitory peptide CaMKIIN (2) in cultured rabbit ventricular myocytes using the cDNA for HA-tagged CAMKIIN (3) inserted into the shuttle vector pacAd5 CMV IRES eGFP pA using the BamH1 and EcoR1 restriction sites. In some cases we dialyzed cells with CaMKIIN peptide (10 μmol/L). The second approach was to infect ventricular myocytes with shRNA against CaMKIIδ inserted into lentivirus, as previously described with minor modifications (4). The shRNA were targeted to a conserved sequence of the mouse and rabbit CaMKIIδ transcript.

Murine CaMKIIδ (accession no. NM_001025438.1) coding sequences were engineered into the pCMV-HA (Clontech Laboratories) to create an N-terminal tag, then shuttled into pCDH lentivector (System Biosciences, SBI). Lentivirus or adenovirus recombination, amplification, and purification were performed by GTVC, as described (4). The cDNA encoding a constitutively active CaMKIIδ (T287D) mutant was created by using the QuikChange Mutagenesis Kit, essentially as described by the manufacturer (Stratagene). The identities of all mutant and WT cDNA sequences were confirmed by sequencing.

Constitutively active CaMKII protein allowed for independent control of "cytoplasmic" (bath) $[Ca^{2+}]_i$ and CaMKII activity, while using Ba^{2+} as the charge carrier in single L-type Ca^{2+} channel (LTCC) recording experiments with cell membrane patches. Monomeric CaMKII (amino acid residues 1–380 of mouse type II, α-isoform) was expressed in baculovirus and purified with a CaM affinity column. The purified CaMKII was made Ca^{2+}-CaM independent by thiophosphorylation of Thr 286 in the presence of Ca^{2+}, CaM, Mg^{2+}, and adenosine 5′-*O*-(3-thiotriphosphate); Ca^{2+}-CaM-independent activity was verified with a phosphorylation assay using a synthetic CaMKII substrate, autocamtide. Constitutively active CaMKII was used at a final concentration of 0.5 μmol/L, to approximate physiological activity (5).

Confocal microscopy and immunofluorescence. Cultured ventricular myocytes on coverslips (glass #1), were paced by field stimulation (Ion Optix C-pace and C-dish, 1 Hz, 35V, 2 ms) for 5 min in Tyrode's solution (1.8 mmol/L $CaCl_2$, 37 °C). Immediately following the pacing protocol, ventricular myocytes were fixed for 20 min in 2% parafomaldyhyde (25 °C). Fixed cells were permeabilized for 10 min with PBS with 0.1% Triton X-100, 2 mg/mL BSA, and 2% fish gelatin. Permeabilized cells were blocked with PBS with 2 mg/mL BSA and 2% fish gelatin. Cells were incubated overnight (4 °C) in one of the following: anti-FLAG conjugated Alexa 488 Ig (Molecular Probes), HA Ig (Santa Cruz), $Ca_V1.2$ [Affinity BioReagents (ABR)], pCaMKII Thr286 Ig (ABR), CaMKII Ig, and washed. The cells incubated with FLAG Ig or $Ca_V1.2$ Ig were then incubated in donkey anti-rabbit Alexa 488 Ig (Molecular Probes) at 4 °C. Cells incubated with pCaMKII Thr286 Ig were then incubated in donkey anti-mouse 568 (Molecular Probes). Cells incubated with CaMKII Ig were then incubated in donkey anti-rabbit 568 (Molecular Probes). Ventricular myocytes were mounted with glass coverslips and Vectashield (with or without DAPI; Vector Laboratories). Ventricular myocyte images were collected on a Zeiss 510 Meta confocal microscope (Carl Zeiss), under 40x magnification (oil, 1.30 N.A. lens), with a pinhole of 1.0 airy disc (Carl Zeiss), using the Zeiss image acquisition software. All images were exported to Photoshop (Adobe) for cropping and linear adjustment of contrast.

Electrophysiology. Voltage and current signals were measured with an Axon 200B patch-clamp amplifier controlled by a personal computer using a Digidata 1320A acquisition board driven by pClamp 8.0 software (Axon Instruments). Electrophysiological recordings were only obtained from Ca^{2+}-tolerant, rod-shaped ventricular cells. We used perforated (amphotericin B) patch for I_{Ca} and action potential studies, according to our previous publications (6), except for excitation-contraction coupling (ECC) gain measurements, where we used conventional whole-cell mode to optimize Ca^{2+} indicator. We used whole-cell mode for sarcoplasmic reticulum (SR) Ca^{2+} content measurements in order to develop conditions to approximately match SR Ca^{2+} content for ECC gain studies (7). All experiments were conducted at $T = 35$ °C. Recording pipettes, fabricated from borosilicate glass, had tip diameters of 2–3 μm and resistance of 2–4 MΩ, when filled with recording solution. All solutions were adjusted to 275–295 mOsm.

Action Potentials. Action potentials were evoked by brief current pulses 1.5–4 pA, 0.5–1 ms. Action potential duration (APD) was assessed as the time from the AP upstroke to 90% repolarization to baseline (APD_{90}). APD_{90} was calculated in the absence of early afterdepolarizations (EADs) unless otherwise noted. EADs were identified as interruptions in the process of AP repolarization, as described (8).

Conventional whole-cell mode voltage clamp studies. The intracellular solution contained (in mmol/L): CsCl 120, $CaCl_2$ 3, tetraethylammonium chloride 10, MgATP 1, NaGTP 1, phosphocreatine 5, Hepes 10, and EGTA 10, titrated to pH 7.2 with 1 mol/L CsOH. The cells were bathed in 137 mmol/L NMDG, 10 mmol/L Hepes,

10 mmol/L glucose, 1.8 mmol/L $CaCl_2$, 0.5 mmol/L $MgCl_2$, and 25 mmol/L CsCl titrated to pH 7.4 with 12.1 mol/L HCl (9).

Perforated patch recordings. APs were recorded using the perforated (amphotericin B) patch-clamp technique (6, 10) at 36 ± 1 °C in Tyrode's solution (bath) with the pipette filled with (mmol/L) 130 potassium aspartate, 10 NaCl, 10 Hepes, 0.04 CaCl2, 2.0 MgATP, 7.0 phosphocreatine, 0.1 NaGTP, and amphotericin B 240 μg/mL, with the pH adjusted to 7.2 with KOH.

SR Ca^{2+} content measurements. SR Ca^{2+} content measurements were performed by integrating the Na^+/Ca^{2+} exchanger currents in response to a "spritz" of caffeine (11). Briefly, cells were held at −80 mV for>5 min for adequate dialysis with pipette solutions before initiating experiments. L-type Ca^{2+} current (I_{Ca}) was activated by stepping the cell membrane from −80 to 0 mV for 300 ms at 0.5 Hz. The bath solution contained (in mmol/L): 137 NaCl, 10 Hepes, 10 glucose, 1.8 $CaCl_2$, 0.5 $MgCl_2$, 25 CsCl, pH was adjusted to 7.4 with NaOH. The intracellular pipette solution contained (in mmol/L): 120 CsCl, 10 tetraethylammonium chloride (TEA), 1.0 MgATP, 1.0 NaGTP, 5.0 phosphocreatine, 10 Hepes, Indo-1 0.2, and pH was adjusted to 7.2 with 1.0 N CsOH. Voltage-activated Na^+ current was inactivated by a 50 ms depolarization step to −40 mV, before completing the depolarization to 0 mV. The K^+ currents were eliminated by adding Cs^+ and TEA and omitting K^+ from the pipette and bath solutions. After loading Ca^{2+} with >15 conditioning command steps, caffeine 20 mmol/L was locally applied by a pipette close to cell of study (DAD-12 Superfusion System, ALA Scientific Instruments.), while cell was holding at −80 mV. The Na^+/Ca^{2+} exchanger currents induced by caffeine were integrated and normalized to cell size. We measured the relationship between the number of conditioning steps and SR Ca^{2+} loading and found that four conditioning steps results in ∼38% SR repletion, while ≥10 conditioning steps results in maximum SR content with 15 prepacing ($n = 3$).

Simultaneous voltage clamp recording of Ca^{2+} current and confocal Ca^{2+} imaging. Simultaneous voltage clamp recording of Ca^{2+} current and confocal Ca^{2+} imaging experiments were performed at 35 °C in ruptured whole-cell configuration. The Ca^{2+} indicator, Fluo-4 pentapotassium salt (100 μmol/L) was dialyzed into the cells in a pipette solution containing (in mmol/L) CsCl 110, TEACl 20, NaCl 10, GTP-Na^+ 0.4, Mg-ATP 5, Hepes 10, $MgCl_2$ 1, pH adjusted to 7.2 with CsOH. The bath solution contained (mmol/L): NaCl 140, KCl 5, $MgCl_2$ 0.5, $CaCl_2$ 1.8, NaH_2PO_4 0.33, glucose 10 and Hepes 10, pH adjusted to 7.4 with NaOH. After establishing whole-cell mode, the cells were switched to recording bath solution containing (mmol/L) NaCl 140, CsCl 10, $MgCl_2$ 1, $CaCl_2$ 1.8, NaH_2PO_4 0.33, glucose 10, Hepes 10, and TTX 0.02, pH 7.4. The cells were clamped to a holding potential of −80 mV. Prior to the test pulses, five (for cells infected with WT β_{2a}) or 10 (for other groups) prepulse stimulations (300 ms at 0 mV from −80 mV, 1 Hz) were applied to approximate similar SR loading amongst treatment groups. We used a ramp depolarization to −40 mV from −80 mV (600 ms) followed by a holding command at −40 mV for 100 ms prior to applying voltage command steps ranging from −30 to +50 mV in 10 mV increments (500 ms). We applied the voltage command at 15 sec intervals. Confocal images were acquired at a sampling rate of 1.92 ms per line (512 pixels per line x 1000 lines), with the scanline along the long axis of the ventricular myocytes.

Single $Ca_V1.2$ channel recordings. Single $Ca_V1.2$ channel recordings were made using two patch-clamp configurations. Cell attached mode recordings were used to estimate the activity of $Ca_V1.2$ in situ. Inside-out recordings from excised cell membrane patches allowed us to apply exogenous, autophosphorylated, and constitutively active CaMKII to the bath (cytoplasmic) solutions. For both cell attached and inside-out configuration recordings the pipette solution contained (mmol/L): $BaCl_2$ 110, Hepes 10, TTX 0.03, and the pH was adjusted with Trizma base to 7.4. LTCC currents were recorded from excised cell membrane patches in response to depolarizing steps to 0 mV (500 ms) from a holding potential −80 mV (0.5 Hz). Nifedipine 100 mmol/L was used at the end of experiments to confirm that recordings were from LTCC currents. The bath solution contained (mmol/L): KCl 150, EGTA 10, Hepes 10, $CaCl_2$ 7.5 or 11, glucose 5.5, EDTA 1, and ATP 0.01; the pH was adjusted to 7.4 with 10 N KOH. For some cell attached studies we used an alternative bath solution—(mmol/L): KCl 145, $MgCl_2$ 2, $CaCl_2$ 0.1, and Hepes 10, with the pH adjusted to 7.4 with KOH. This alternate solution contained 0.1 mmol/L Ca^{2+} to reduce the possibility of intracellular Ca^{2+} depletion. However, we did not detect differences in LTCC currents recorded using either bath solution. Currents were sampled at 20 kHz and low-pass filtered at 2 kHz using a four-pole Bessel filter. Only patches containing a single Ca^{2+} channel were analyzed. All single-channel recordings were analyzed using Clampfit10 software. We estimated the Po for each active sweep and estimated the open times with Gaussian or two-exponential fits. The dwell-time histograms where time values were plotted on a log scale were fitted as a Gaussian distribution. When the time value was plotted on a linear scale the data were fit with two exponentials. Modal gating analysis was performed as previously described. (12, 13)

Cell pacing and viability measurements. Dissociated ventricular myocytes were cultured on 12-mm-diameter (glass #1) cover glasses placed into four-well Nunclon Delta Treated dishes (10 coverslips in each well). We used morphology and Trypan blue staining to estimate cell viability (13). Prior to pacing (after 24 h in culture in the presence of adenovirus) and at each other time point, 2–3 coverslips were taken from each well and exposed to 0.1% Trypan blue dissolved in normal Tyrode solution for 5 min. The number of stained and unstained cells was counted on five randomly chosen fields of view on a coverslip at 200x (Olympus, CK 2). Cultured ventricular myocytes were paced up to 24 h by field stimulation (Ion Optix C-pace and C-dish, 1 Hz, 35 V, 2 ms) in Hank's Balanced Salt Solution (1 mmol/L $CaCl_2$, 37 °C). Cell suspensions were concentrated by centrifugation (1 min /75 g) and a 25 μL aliquot of the cell pellet was mixed with an equal volume of counting media (1% glutaraldehyde in modified Tyrode's solution containing 1% Trypan blue). The cells were examined microscopically at 100x magnification to determine the morphology (rod, round, or square) and the permeability of these cells to Trypan blue. Viable cells were analyzed as cells with a rod-shaped morphology and a length/width ratio of more than 3/1 and expressed as a percentage of total cells counted. The total count always exceeded 50 cells and was completed within 15 min to preclude nonspecific uptake of Trypan blue by the cells.

Mathematical modeling. The model was updated to include dynamic activation of CaMKII by Ca^{2+}/calmodulin and downstream regulation of I_{Ca}, SR Ca^{2+} release, and SR Ca^{2+} uptake (14, 15). Mode 2 gating was simulated as in Tanskanen et al., by decreasing the rate constant for the transition from the open state to first closed state by a factor of 10 (16). The fraction of mode 2 channels was made a function of CaMKII activity. β_{2a} expression was simulated by increasing peak I_{Ca} by a factor of two. The T498A β_{2a} mutant was simulated by eliminating the effect of CaMKII on the LTCC (peak Ca^{2+} current increase was the same as WT). The models were paced to steady-state at a cycle length of 1 Hz.

Complete LRd equations and definitions may be found in a previous publication (17). Here we provide equations and parameters that differ from the original model.

L-type Ca^{2+} current, $I_{Ca(L)}$.
We use the L-type Ca^{2+} channel Markov model developed by Faber et al. (17) with the following modifications to account for CaMKII regulation of mode 2 gating and channel inactivation. Mode 2 gating is simulated by decreasing the rate constant for the transition from the open state to first closed state (β_3) by a factor of 10 (16).

Mode 2 gating:

$$\beta_3 = 0.4 \cdot \beta$$

$$\beta = 0.39 \cdot \exp(-V_m/40)$$

$$\text{Fraction of Mode 2 channels} = \bar{\Delta}\text{frac}_{M2,CamK}/(1 + (K_{m,CaMK}/CaMKII_{\text{active}})^h)$$

$$\bar{\Delta}\text{frac}_{M2,CaMK} = 0.3; \qquad K_{m,CaMK} = 0.04; \qquad h = 5.0$$

$$\phi_f = (0.02 - \Delta\phi_{f,CaMK}) \cdot \exp(V_m/500)$$

$$\Delta\phi_{f,CaMK} = \bar{\Delta}\phi_{f,CaMK}/(1 + (K_{m,CaMK}/CaMKII_{\text{active}})^h)$$

$$\bar{\Delta}\phi_{f,CaMK} = 0.015; \qquad K_{m,CamK} = 0.05; \qquad h = 5.0$$

$$\phi_s = (0.03 - \Delta\phi_{s,CaMK}) \cdot \exp(V_m/-280)$$

$$\Delta\phi_{s,CaMK} = \bar{\Delta}\phi_{s,CaMK}/(1 + (K_{m,CaMK}/CaMKII_{\text{active}})^h)$$

$$\bar{\Delta}\phi_{s,CaMK} = 0.005; \qquad K_{m,CaMK} = 0.05; \qquad h = 5.0$$

To simulate β_{2a} mutant activity, $\bar{\Delta}\text{frac}_{M2,CaMK} = \bar{\Delta}\phi_{f,CaMK} = \bar{\Delta}\phi_{s,CaMK} = 0.0$.

To simulate β_{2a} WT or mutant overexpression, $P_{Ca} = 0.0126$ cm/s.

SR Ca^{2+} release, I_{rel}.

$$\gamma_{5R} = (8.4 - \Delta\gamma_{5R,CaMK}) \cdot [Ca^{2+}]_{ss}$$

$$\Delta\gamma_{5R,CaMK} = \bar{\Delta}\gamma_{5R,CaMK}/(1 + (K_{m,CaMK} + CaMKII_{\text{active}})^h)$$

$$\bar{\Delta}\gamma_{5R,CaMK} = 5.0; \qquad K_{m,CaMK} = 0.05; \qquad h = 5.0$$

SR Ca^{2+} uptake, I_{up}.
The mathematical formulation for CaMKII regulation of SR Ca^{2+} uptake by is taken from our previous publications (15, 16):

$$I_{\text{up}} = \bar{I}_{\text{up}} \cdot \frac{[Ca^{2+}]_i}{[Ca^{2+}]_i + K_{m,up} - \Delta K_{m,PLB,CaMK}}$$

$$\Delta K_{m,PLB,CaMK} = \bar{\Delta} K_{m,PLB,CaMK}/(1 + (K_{m,CaMK}/CaMKII_{\text{active}})^h)$$

$$\bar{\Delta} K_{m,PLB} = 0.00017 \text{ mmol/L}; \qquad K_{m,CaMK} = 0.05;$$
$$h = 5.0; \qquad \bar{I}_{\text{up}} = 0.017325$$

CaMKII.
The mathematical equations describing CaMKII activity are the same as published previously (15, 16):

$$CaMKII_{\text{bound}} = CaMKII_o \cdot (1 - CaMKII_{\text{trap}})/(1 + K_{m,CaMK}/[Ca^{2+}]_{ss})$$

$$\frac{dCaMKII_{\text{trap}}}{dt} = \alpha_{CaMK} \cdot CaMKII_{\text{bound}} \cdot (CaMKII_{\text{bound}} + CaMKII_{\text{trap}}) - \beta_{CaMK} \cdot CaMKII_{\text{trap}}$$

$$CaMKII_{\text{active}} = CaMKII_{\text{bound}} + CaMKII_{\text{trap}}$$

$$\alpha_{CaMK} = 0.0006 \text{ ms}^{-1}; \qquad \beta_{CaMK} = 0.00003 \text{ ms}^{-1}$$

$$CaMKII_o = 0.05; \qquad K_{m,CaM} = 0.001 \text{ mmol/L}$$

1. Grueter CE, et al. (2006) L-type Ca2+ channel facilitation mediated by phosphorylation of the beta subunit by CaMKII. *Mol Cell*, 23:641–650.
2. Chang BH, Mukherji S, Soderling TR (1998) Characterization of a calmodulin kinase II inhibitor protein in brain. *Proc Natl Acad Sci USA*, 95:10890–10895.
3. Singh MV, et al. (2009) Ca2+/calmodulin-dependent kinase II triggers cell membrane injury by inducing complement factor B gene expression in the mouse heart. *J Clin Invest*, 119:986–996.
4. Erickson JR, et al. (2008) A dynamic pathway for calcium-independent activation of CaMKII by methionine oxidation. *Cell*, 133:462–474.
5. Gupta RC, Kranias EG (1989) Purification and characterization of a calcium-calmodulin-dependent phospholamban kinase from canine myocardium. *Biochemistry*, 28:5909–5916.
6. Wu Y, et al. (2009) Calmodulin kinase II is required for fight or flight sinoatrial node physiology. *Proc Natl Acad Sci USA*, 106:5972–5977.
7. Chen B, Wu Y, Mohler PJ, Anderson ME, Song LS (2009) Local control of Ca2+-induced Ca2+ release in mouse sinoatrial node cells. *J Mol Cell Cardiol*, 47:706–715.
8. Wu Y, MacMillan LB, McNeill RB, Colbran RJ, Anderson ME (1999) CaM kinase augments cardiac L-type Ca2+ current: A cellular mechanism for long Q-T arrhythmias. *Am J Physiol*, 276:H2168–H2178.
9. Wu Y, Dzhura I, Colbran RJ, Anderson ME (2001) Calmodulin kinase and a calmodulin-binding "IQ" domain facilitate L-type Ca2+ current in rabbit ventricular myocytes by a common mechanism. *J Physiol*, 535:679–687.
10. Rae J, Cooper K, Gates P, Watsky M (1991) Low access resistance perforated patch recordings using amphotericin B. *J Neurosci Methods*, 37:15–26.
11. Zhang R, et al. (2005) Calmodulin kinase II inhibition protects against structural heart disease. *Nat Med*, 11:409–417.
12. Dzhura I, Wu Y, Colbran RJ, Balser JR, Anderson ME (2000) Calmodulin kinase determines calcium-dependent facilitation of L-type calcium channels. *Nat Cell Biol*, 2:173–177.
13. Chen X, et al. (2005) Ca2+ influx-induced sarcoplasmic reticulum Ca2+ overload causes mitochondrial-dependent apoptosis in ventricular myocytes. *Circ Res*, 97:1009–1017.
14. Hund TJ, et al. (2008) Role of activated CaMKII in abnormal calcium homeostasis and INa remodeling after myocardial infarction: Insights from mathematical modeling. *J Mol Cell Cardiol*, 45:420–428.
15. Hund TJ, Rudy Y (2004) Rate dependence and regulation of action potential and calcium transient in a canine cardiac ventricular cell model. *Circulation*, 110:3168–3174.
16. Tanskanen AJ, Greenstein JL, O'Rourke B, Winslow RL (2005) The role of stochastic and modal gating of cardiac L-type Ca2+ channels on early afterdepolarizations. *Biophys J*, 88:85–95.
17. Faber GM, Silva J, Livshitz L, Rudy Y (2007) Kinetic properties of the cardiac L-type Ca2+ channel and its role in myocyte electrophysiology: A theoretical investigation. *Biophys J*, 92:1522–1543.

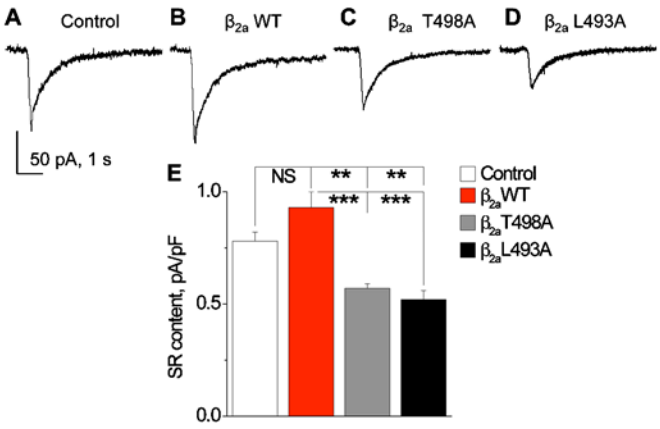

Fig. S1. SR Ca^{2+} content is higher in β_{2a} WT infected cardiomyocytes ($n = 13$) compared to β_{2a} T498A ($n = 9$) and L493A ($n = 10$) infected cardiomyocytes. (*A–D*) Representative caffeine-evoked Na^{+}/Ca^{2+} exchanger current recordings. (*E*) Summary data show increased SR content in β_{2a} WT infected cardiomyocytes compared to β2a T498A and β2a L493A expressing cells ($^{**}P < 0.01$, $^{***}P < 0.001$).

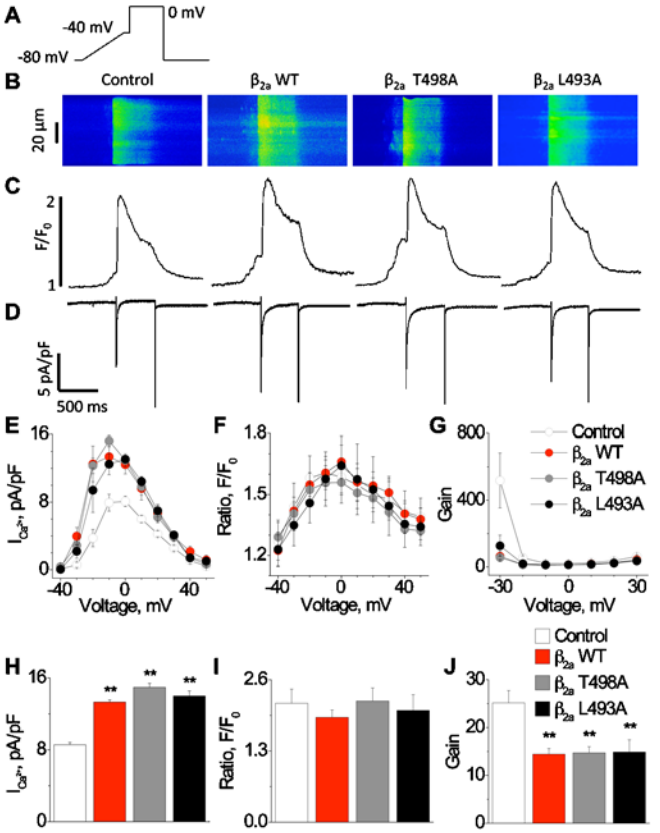

Fig. S2. ECC gain is equivalent after infection with WT or mutant β_{2a} subunits. (*A*) Voltage command protocol used to evoke I_{Ca} and trigger SR Ca^{2+} release, as shown in *B–D*. (*B*) Representative intracellular Ca^{2+} transients triggered by a depolarizing pulse to 0 mV. (*C*) Spatially averaged intracellular Ca^{2+} transient profiles from confocal images shown in *B*. (*D*) I_{Ca} recorded simultaneously with the intracellular Ca^{2+} transients in *B*. (*E–G*) Peak I_{Ca}, peak intracellular Ca^{2+} transient amplitude (F/Fo), and the ECC gain (calculated as the ratio of the peak Ca^{2+} transient/peak $I_{Ca} \times 100$). (*H–J*) Summary data for peak I_{Ca}, peak intracellular Ca^{2+} transient, and ECC gain in response to a depolarizing step to 0 mV. ECC gain was not different in myocytes transfected with WT β2a or mutant β2a (T498A, L493A).

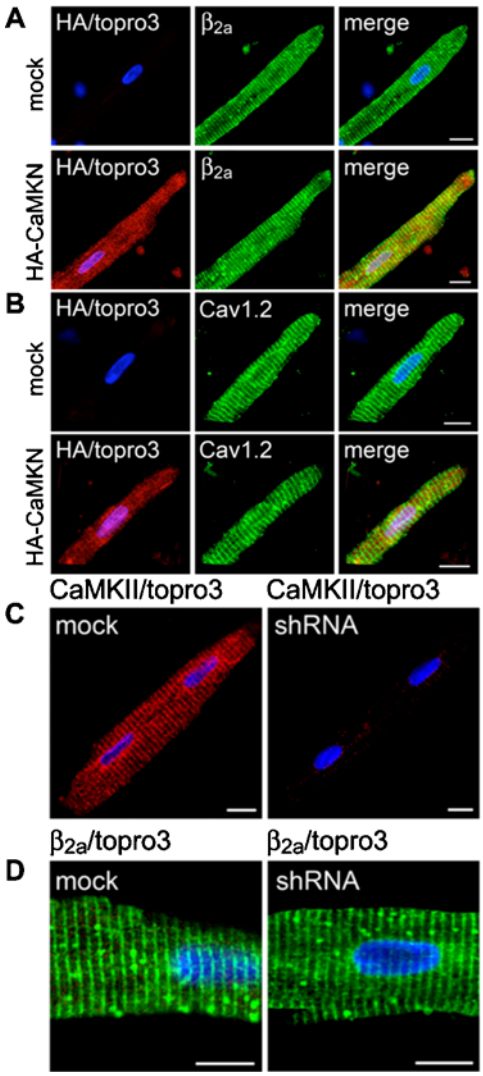

Fig. S3. CaMKIIN expression and shRNA knockdown of CaMKIIδ are effective and do not affect expression of exogenous β_{2a} or endogenous $Ca_V1.2$. Confocal immunofluorescent images show HA epitope detection of the CaMKII inhibitor peptide CaMKIIN (red staining, *Left*), FLAG epitope detection of WT β_{2a} (green staining, *Middle* in *A*), or $Ca_V1.2$ (green staining, *Middle* in *B*), and merged images (*Right*). Blue staining is for the nuclear dye topro-3. Confocal immunofluorescent micrographs show (*C*) CaMKII staining (*Red*) that is nearly eliminated by shRNA. (*D*) shRNA does not affect expression of FLAG-tagged WT β_{2a} subunits. Blue staining is nuclear dye topro-3. (Calibration bar: 10 μm.)

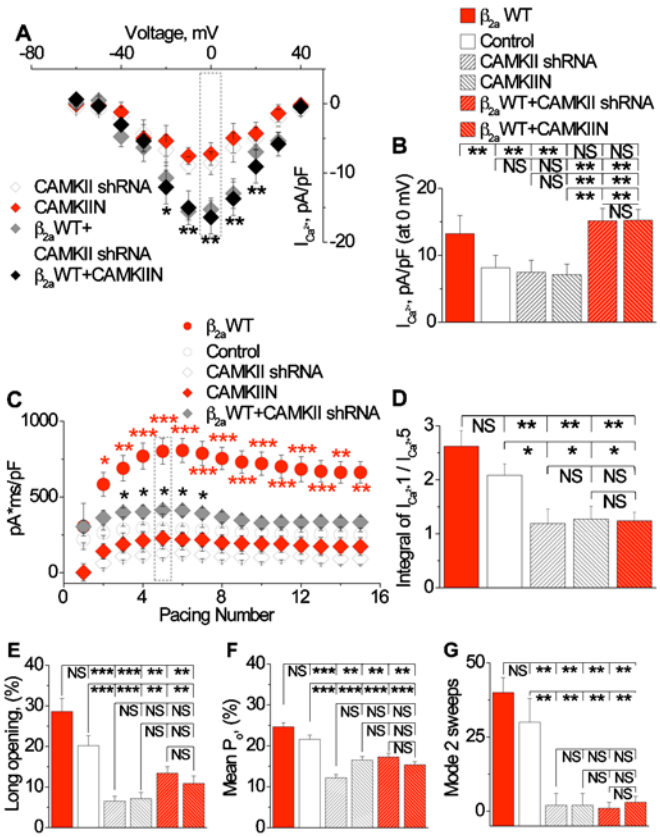

Fig. S4. Global cellular CaMKII inhibition prevents I_{Ca} facilitation and mode 2 gating. (*A*) Current-voltage relationship for I_{Ca} recorded from ventricular myocytes with CaMKII inhibition by shRNA knockdown or expression of the inhibitory peptide CaMKIIN. Cells with β_{2a} WT expression and CaMKII inhibition have significantly (** $P < 0.01$) increased peak I_{Ca} compared to cells with CaMKII inhibition and no β_{2a} WT expression. (*B*) Peak I_{Ca} density in response to a voltage command pulse to 0 mV (data from *A*). The vertical ticks mark groups for statistical comparison as in Fig. 1*F*. (*C*) Summary data for integrated I_{Ca} in response to a train of 15 voltage command pulses from the same experimental groups shown in *A*. (*D*) Integrated I_{Ca} for the fifth command pulse divided by the first command pulse from *C*. *E*–*G* show summary data for single LTCC channel currents from the same groups as in *A*, arranged as in panels *G*–*I* for Fig. 2. Each group represents data from 10–12 cells for whole-cell mode and 8–10 cells for recordings of single-channel activity The vertical ticks mark groups for statistical comparison as in Fig. 1*F*.

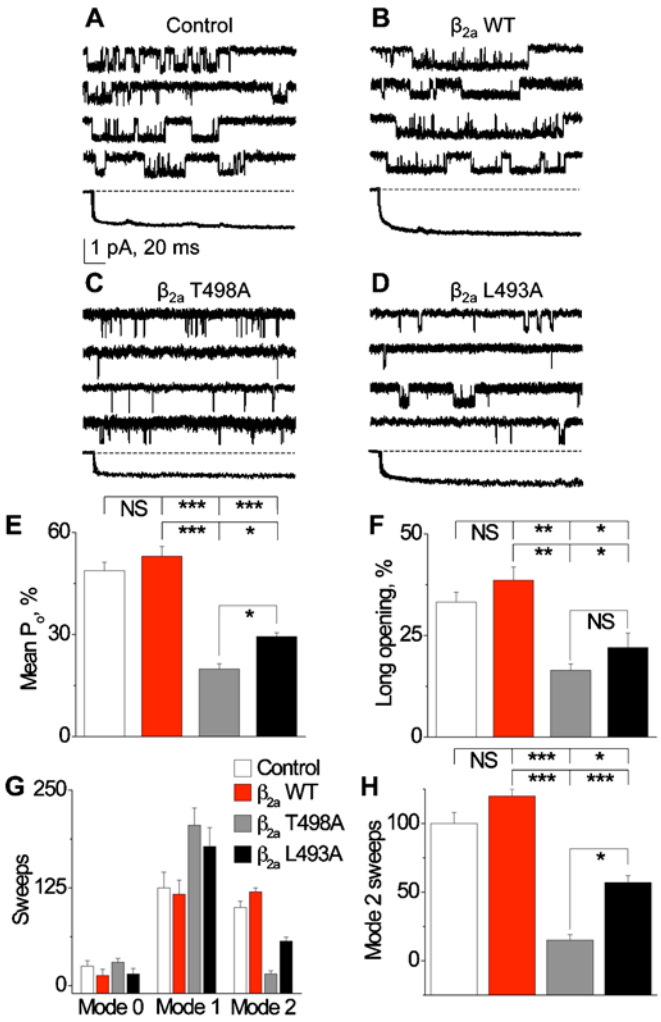

Fig. S5. CaMKII phosphorylation and binding sites are crucial for CaMKII activation of single LTCCs recorded from excised cell membrane patches. (*A–D*) Example single LTCC recordings from each of the experimental groups in the presence of autophosphorylated CaMKII (0.5 μM) added to the bath (cytoplasmic) solution. (*E*) Mean opening probability (P_o); (*F*) percent of long LTCC openings; (*G* and *H*) mode 2 gating events are significantly reduced in β_{2a} T498A and L493A reconstituted LTCCs compared to LTCCs recorded in membrane patches excised from β_{2a} WT or mock-infected ventricular myocytes in the presence of autophosphorylated CaMKII (0.5 μM) added to the bath (cytoplasmic) solution. The vertical ticks mark groups for statistical comparison as in Fig. 1*F*. $^{*}P < 0.05$; $^{**}P < 0.01$, $^{***}P < 0.001$ versus empty vector controls. Each experimental group represents 8–10 cells.

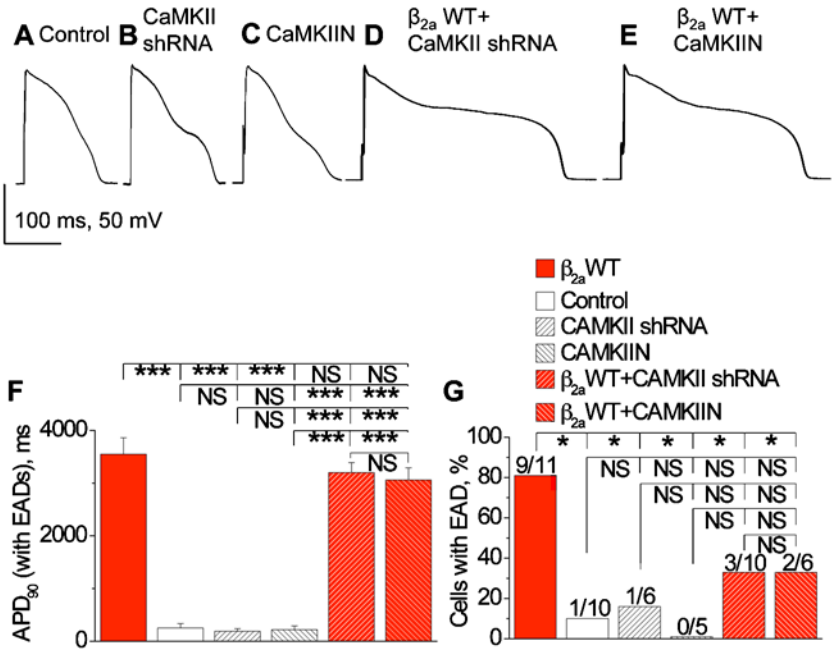

Fig. S6. Global cellular CaMKII inhibition inhibits EADs without shortening APD. (*A–E*) Representative action potentials from ventricular myocytes expressing the labeled proteins and/or shRNA. (*F*) Summary data showing APD prolongation by β_{2a} WT is not diminished by CaMKII inhibition. (*G*) CaMKII inhibition provides similar protection against EADs in the presence or absence of β_{2a} WT expression. The vertical ticks mark groups for statistical comparison ($^{*}P < 0.05$, $^{***}P < 0.001$). All cells in *G* were used for APD measurements in *F*.

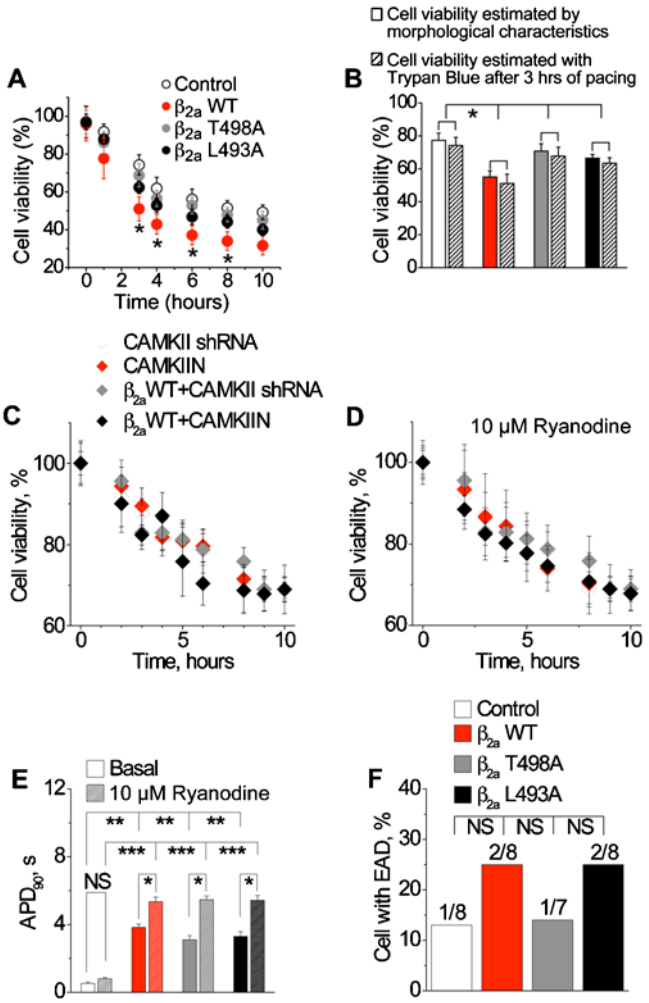

Fig. S7. Reduced cardiomyocyte survival by β_{2a} WT infection is rescued by CaMKII inhibition. (*A*) Summary data for cell viability based on Trypan blue exclusion. (*B*) Comparison of morphological and Trypan blue exclusion assessment of cell viability. Each data point is from an average of ≥50 cells. $^{*}P < 0.05$ compared to vector-infected controls by either method. (*C*) CaMKII inhibition by shRNA knock down or CaMKIIN expression protects against premature cell death equivalently in β_{2a} WT expressing or mock-infected cells. (*D*) Ryanodine treatment confers no additional protection to CaMKII inhibited cells. The vertical ticks mark groups for statistical comparison as in Fig. 1*F*. (*E*) Ryanodine significantly and equivalently prolongs the APD in β_{2a} WT, β_{2a} T498A, and β_{2a} L493A groups. (*F*) Ryanodine treatment prevents increased EAD induction by β_{2a} WT infection (compare to Fig. 2*F*). The vertical ticks mark groups for statistical comparison as in Fig. 1*F*. $^{*}P < 0.05$, $^{**}P < 0.01$, $^{***}P < 0.001$ versus empty vector controls. Each experimental group represents 10–12 cells.

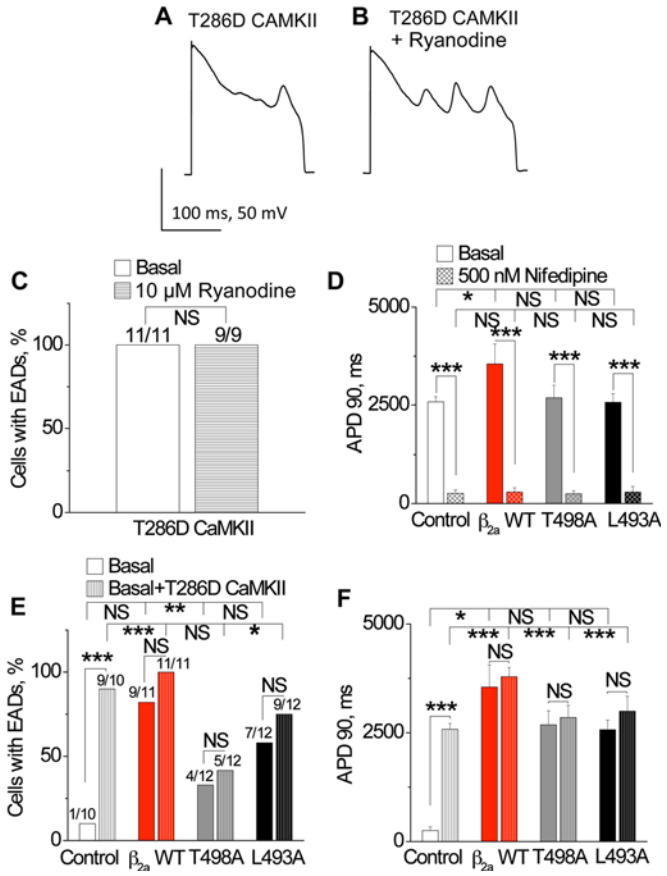

Fig. S8. EADs persist after ryanodine in myocytes infected with constitutively active CaMKII. Representative action potentials from ventricular myocytes infected with constitutively active CaMKII (T286D) in (*A*) control conditions and (*B*) after 10 μM ryanodine. Ryanodine treatment conditions were the same as in Fig. S7*F*). (*C*) Summary data showing T286D CaMKII overexpression induced EADs in 100% of cells and 10 μM Ryanodine did not abolish this effect. (*D*) 500 nM Nifedipine significantly and equivalently decreased APD_{90} in all groups. $^{***}P < 0.001$. (*E*) β_{2a} T498A overexpression significantly reduced the efficacy of EAD induction by T286D CaMKII expression (*F*) without significant changing APD_{90}.

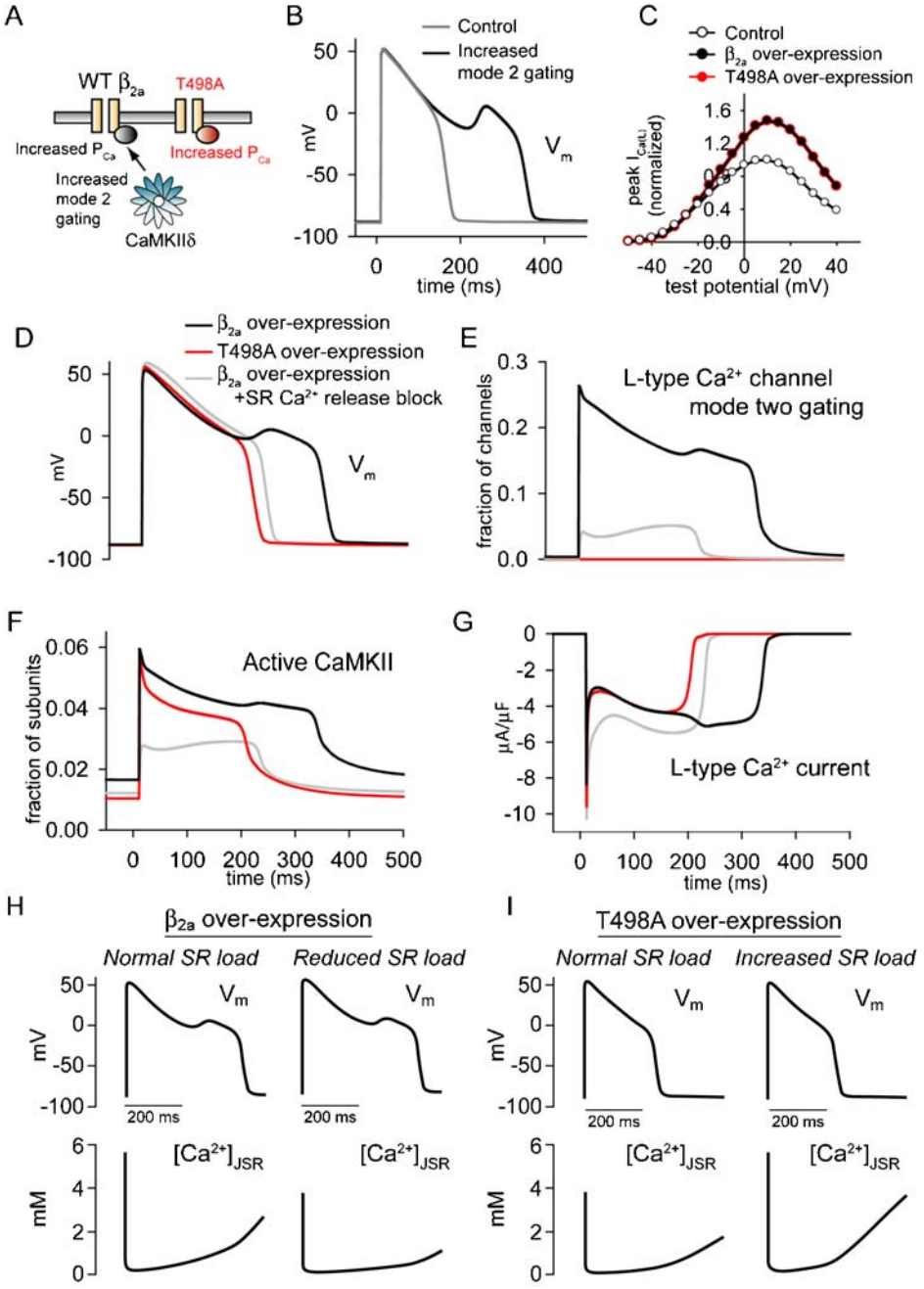

Fig. S9. Calmodulin kinase II generates early afterdepolarizations in myocytes overexpressing β_{2a}: Insights from mathematical modeling. (*A*) Mathematical model of β_{2a} overexpression assumes that I_{Ca} membrane permeability (P_{Ca}) is increased due to overexpression of either WT or mutant (T498A) β_{2a} subunit. However, only the WT subunit may be regulated by CaMKII activity. (*B*) An increase in mode 2 gating alone may produce afterdepolarizations in a computer model of the cardiac action potential (fraction of channels showing mode 2 gating = 0.48, *black line*). Simulation results are shown after pacing to steady state at 1000 ms cycle length. (*C*) Simulated L-type Ca^{2+} current-voltage relationship for WT β_{2a} and T498A mutant overexpression models compared to control (untransfected). Total L-type Ca^{2+} channel permeability is increased twofold in both the WT and T498A mutant overexpression models to simulate increased trafficking of functional channels. Total CaMKII activity held at zero during voltage clamp simulations. (*D*) Simulated action potentials, (*E*) CaMKII activity, (*F*) fraction of mode 2 L-type Ca^{2+} channels, and (*G*) L-type Ca^{2+} current in a mathematical model of WT β_{2a} overexpression (*black lines*), T498A mutant overexpression (*red*), and WT β_{2a} overexpression in the presence of SR Ca^{2+} release block (*gray*). Simulation results are shown after pacing to steady state at 1000 ms cycle length. Note the presence of an early afterdepolarization in the β_{2a} overexpression model but not in the T498A mutant. β_{2a} overexpression results in greater CaMKII activity during the action potential plateau compared to T498A mutant. Increased CaMKII activity, in turn, promotes mode 2 gating and reactivation of the L-type Ca^{2+} current during the plateau that produces an EAD. Block of SR Ca^{2+} release decreases CaMKII activity, reduces the number of channels exhibiting mode 2 gating, and eliminates the early afterdepolarization. (*H* and *I*) To determine whether afterdepolarization observed in the β_{2a} overexpression model depend on increased SR Ca^{2+} load, simulated action potentials and junctional SR [Ca^{2+}] are shown at steady state (normal SR load) or with the SR load altered immediately before the final stimulus. Afterdepolarizations occur in the simulated β_{2a} overexpression action potential even if SR [Ca^{2+}] is transiently reduced to the steady-state value from the T498A model. Likewise, afterdepolarizations are not observed in the simulated T498A action potential even if SR [Ca^{2+}] is increased to WT levels. Thus, the model predicts that increased likelihood of afterdepolarization formation observed with β_{2a} overexpression is not due to differential loading of the SR.